This is a repository copy of *A nonlinear spring mechanism incorporating a bistable composite plate for vibration isolation*.

White Rose Research Online URL for this paper:
http://eprints.whiterose.ac.uk/80840/

Version: Submitted Version

Article:
Shaw, A.D., Neild, S.A., Wagg, D. et al. (2 more authors) (2013) A nonlinear spring mechanism incorporating a bistable composite plate for vibration isolation. Journal of Sound and Vibration, 332 (24). 6265 - 6275. ISSN 0022-460X

https://doi.org/10.1016/j.jsv.2013.07.016

Reuse
Unless indicated otherwise, fulltext items are protected by copyright with all rights reserved. The copyright exception in section 29 of the Copyright, Designs and Patents Act 1988 allows the making of a single copy solely for the purpose of non-commercial research or private study within the limits of fair dealing. The publisher or other rights-holder may allow further reproduction and re-use of this version - refer to the White Rose Research Online record for this item. Where records identify the publisher as the copyright holder, users can verify any specific terms of use on the publisher's website.

Takedown
If you consider content in White Rose Research Online to be in breach of UK law, please notify us by emailing eprints@whiterose.ac.uk including the URL of the record and the reason for the withdrawal request.

eprints@whiterose.ac.uk
https://eprints.whiterose.ac.uk/

A nonlinear spring mechanism incorporating a bistable composite plate for vibration isolation

A. D. Shaw[a,*], S. A. Neild[b], D. J. Wagg[b], P. M. Weaver[a], A. Carrella[c]

[a] *Advanced Composites Centre for Science and Innovation (ACCIS), University of Bristol, Queen's Building, Bristol, BS8 1TR, United Kingdom*
[b] *Department of Mechanical Engineering, University of Bristol, Queen's Building, Bristol, BS8 1TR, United Kingdom*
[c] *LMS International, Researchpark Z1, Interleuvenlaan 68, 3001 Leuven, Belgium*

Abstract

The High Static Low Dynamic Stiffness (HSLDS) concept is a design strategy for a nonlinear anti-vibration mount that seeks to increase isolation by lowering the natural frequency of the mount whilst maintaining the same static load bearing capacity. It has previously been proposed that an HSLDS mount could be implemented by connecting linear springs in parallel with the transverse flexure of a composite bistable plate — a plate that has two stable shapes between which it may snap. Using a bistable plate in this way will lead to lightweight and efficient designs of HSLDS mounts. This paper experimentally demonstrates the feasibility of this idea. Firstly, the quasi-static force-displacement curve of a mounted bistable plate is determined experimentally. Then the dynamic response of a nonlinear mass-spring system incorporating this plate is measured. Excellent agreement is obtained when compared to theoretical predictions based on the measured force-displacement curve, and the system shows a greater isolation region and a lower peak response to base excitation than the equivalent linear system.

Keywords: Vibration Isolation, Nonlinear Dynamics, HSLDS, Bistable, Composites

*Corresponding author

1. Introduction

Vibration isolation is a vital requirement throughout much of engineering [1], particularly when there is a strong source of vibration such as a motor. It is frequently required to prevent the transmission of these vibrations to other elements of the system, for reasons such as passenger comfort, or the protection of delicate electronic equipment.

A High Static Low Dynamic Stiffness (HSLDS) mount seeks to improve vibration isolation by reducing the natural frequency of the mount and its payload, whilst maintaining the weight bearing capacity of the mount [2]. In the current work, a nonlinear spring mass system, with an HSLDS force-displacement relationship, is subjected to harmonic base excitation and response is compared to analytical predictions made by [3].

An HSLDS response is often achieved by the parallel connection of linear springs with a snap-through mechanism providing a region of negative stiffness [4], and this approach is followed here. The chosen negative stiffness device is the transverse displacement of the centre of a composite bistable plate. Bistable plates of this kind have two stable equilibrium shapes which they may snap between [5], as shown in Fig. (1) (a) and (c). By holding the plate at the unstable position between these two equilibria shown in Fig. (1) (b), negative stiffness is observed, which is used to tailor the force-displacement response. This approach was proposed by Carrella and Friswell [6]. It is thought that the use of flexible composite shells instead of potentially complex spring mechanisms could lead to lightweight and efficient implementations of the HSLDS concept.

Isolators that exhibit HSLDS behaviour are numerous in the literature, although the HSLDS term itself is relatively new. Authors such as Winterflood [7], Virgin and Davis [8], Plaut et al. [9], Santillan [10, 11], DeSalvo [12], Carrella et al. [13, 14, 15], Kovacic et al. [16], Zhou and Liu [17], Robertson et al. [18], and Le and Ahn [19] have all worked on variations of the HSLDS concept. Furthermore, many HSLDS devices are found in the review of passive vibration isolation methods by Ibrahim [4]. General analysis of the nonlinear phenomena

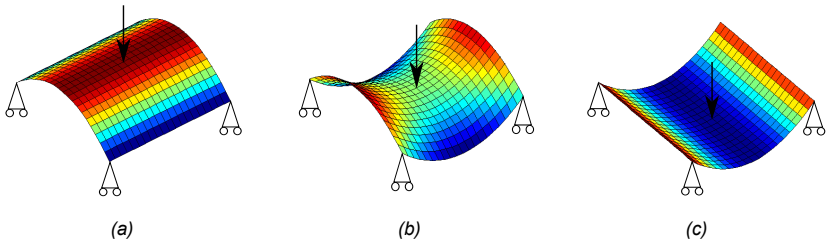

Figure 1: The different stages of the transverse force-through of a bistable state. (a) Initial, approximately singly curved configuration. (b) At mid point of force through the plate is a saddle shape; this shape is unstable if unconstrained and at this point the force displacement graph has negative slope. (c) Final singly curved configuration with curvature along perpendicular axis to initial curvature.

encountered by HSLDS mounts including amplitude dependant transmissibility and jump frequencies, based on Duffing oscillator models are given in [2]. Shaw *et. al.* has also recently published an analytical study of the HSLDS, showing the significant effect that subtle differences in the shape of the nonlinear force displacement relationship can cause, and proposing two nondimensional parameters, which can characterise many HSLDS systems [3].

The 'snapping' response of bistable plates was first reported and analysed by Hyer [5, 20]. He also proposed that these effects could be exploited for the purpose of actuation, creating a device that could occupy multiple configurations with no ongoing power consumption. Since then, there has been considerable interest in bistability, for example many authors have looked towards implementing bistable plates in morphing aerodynamic devices including Diaconu *et. al.* [21], Schultz [22], Gatto *et. al.* [23], Daynes *et. al.* [24, 25] and Lachenal *et. al.* [26].

In the current work, the principal aspect of the bistable plate that is of concern is the response to external loading, particularly within the region between the plates two stable states. This has previously been considered by Dano and Hyer [27], Potter *et. al.* [28], Tawfik [29], Diaconu *et. al.* [30], Pirrera *et. al.* [31] and Shaw *et. al.* [32]. However, the current work demonstrates that substantial qualitative differences to the force displacement curves found in these

works may be obtained.

Section 2 of this work proceeds with a description of the bistable plate, how it was mounted, and its experimentally derived nonlinear force-displacement curve. Section 3 then describes the dynamic experiment that was conducted. Section 4 gives a summary of the key static and dynamic features of an HSLDS mount, and Section 5 compares the experimental results with theory. Conclusions are drawn in Section 6.

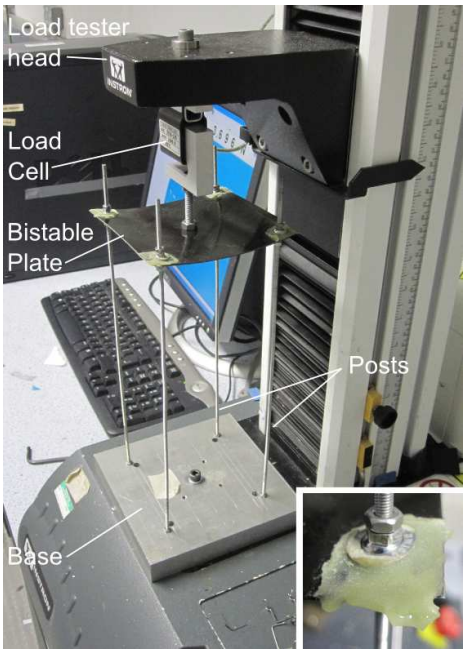

Figure 2: The assembled quasi-static test rig. Inset shows detail of one of the spherical pivot joints used to mount corners.

2. Quasi-static response of the mounted bistable plate subjected to transverse centre loading

2.1. Bistable plate

A composite bistable plate is typically created on flat tooling by using a stacking sequence of unidirectional carbon fibre reinforced plastic (CFRP) plies that is asymmetric about the midplane of the plate. The directional thermal expansion properties of the plies cause the plate to warp as it cools from its cure temperature to room temperature, and nonlinear geometrical effects cause the snapping phenomenon [20].

Hybrid composite bistable plates, consisting of CFRP and steel ply layers, have been shown to give much greater snapping forces than all CFRP plates [33]. To allow a more compact configuration, this type of plate is used here. The layup and dimensions were chosen to give relatively low curvature in each bistable

state, to prevent the plate forming 'half-snap' states during snap-through as reported in [28, 31, 30, 32], which would cause an undesired non-smooth response. The selected configuration was a 110 mm square plate with a layup $[0^{\circ}_{3CF}$, 0°_{1S} , $90^{\circ}_{3CF}]$, where the subscripts indicate the number of plies along with CF for plies of IM7/8552 Intermediate Modulus Carbon Fibre pre-preg nominally 0.125 mm thick, and S for a steel ply 0.25 mm thick. The steel ply was lightly abraded to improve 'wetting' properties and thereby enhance its bonding with the pre-preg layers. It was vacuum bagged using a tool plate on both sides, to ensure the most symmetrical resin distribution through thickness. It was cured using the manufacturers recommended cycle in an autoclave at 180°C for 2 hours. Holes 12 mm in diameter were drilled 10 mm in from each corner, to accommodate pivot joints described below.

2.2. Mounting mechanism

The plate was supported by its corners, on apparatus designed to provide boundary conditions which do not restrain the snap through. These corner boundary conditions are vertical pins i.e they allow free out of plane rotation, zero vertical displacement and free lateral translation. To achieve the first of these conditions, the corners were fitted with spherical bearings that were bonded into the 12 mm holes drilled through the plate, that permitted pivoting in any direction. The plate was clamped flat for the bonding of the pivot joints, so that the glue fillets did not set into the shape of either stable configuration. To simultaneously achieve the second and third boundary conditions, the bearings were mounted on tall slender steel posts (approximately 250 mm long, 3 mm in diameter), which were rigidly attached to an adjustable base. Clearly a more compact mounting would be desirable in a practical design, but this would cause some compromise to the ideal boundary conditions sought here for the purpose of establishing feasibility. Vertically the posts provided stiffness greatly in excess of the plate's transverse stiffness, and could withstand sufficient buckling force. Horizontally, the posts acted as soft cantilever springs, and the size of lateral motions was not sufficient to cause significant vertical deflections.

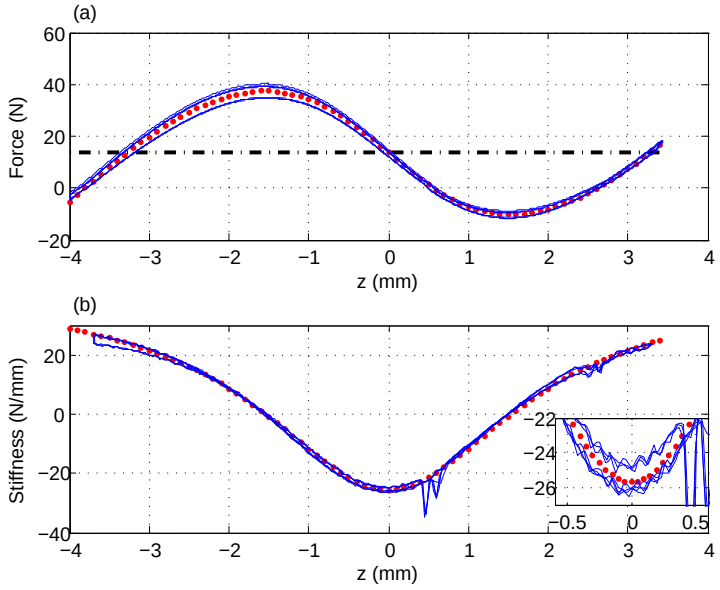

Figure 3: (a) Force-displacement response for plate mounting. Solid lines show results from quasi-static force-displacement test. Dotted lines show fitted function. Dot-dashed line shows offset axis about which response is approximately an odd function. (b) Stiffness-displacement response for plate mounting. Dotted lines show fitted function.

2.3. Quasi-static response

The above apparatus was bolted onto an Instron 3343 load tester, with the centre of the plate bolted to a 1kN load cell. The complete apparatus is shown in Fig. (2). The displacement cycle applied to the plate consisted of increasing displacement at constant velocity over a range including both stable positions of the plate, then returning at the same speed to the starting point. This was performed 4 times to ensure repeatability, at a speed of 6 mm/min. Fig. (3) (a) shows the results of the quasi-static test. There is a small amount of hysteresis in each cycle, which we believe are caused by frictional moments within the corner bearings. There is also a large asymmetry in the cycle; the maximum positive force is greater in magnitude than the minimum negative force. This asymmetry is caused by stresses locked in by the adhesive fillets used to attach the corner

joints, and other manufacturing imperfections. The asymmetry takes the form of a vertical offset; the dot-dashed line in the graph at F=13.5 N illustrates the line around which the response is approximately an odd function, as required by our HSLDS analysis.

Ignoring hysteresis and correcting for the vertical offset, the response may be fitted with the following function:

$$F = Az - B\arctan(Cz) \tag{1}$$

where $A = 41.9$, $B = 133.3$ and $C = 0.507$. The coefficients are found by solving such that the displacement at the zero crossings, the peak force, and the displacement at peak force match graph readings. As the dotted line in Fig. (3) (a) shows, this gives a good representation of the central shape of the data.

For dynamic purposes, the stiffness-displacement profile is often of greater concern than the force-displacement profile. Fig. (3) (b) shows the stiffness-displacement profile, calculated by numerically differentiating the force-displacement data with regard to displacement. An undesirable spike occurs at approximately z=0.5 mm. This is caused by a small degree of freeplay within one of the spherical joints causing a discontinuity as their loading changes sign. Eq. (1) differentiates to

$$\frac{dF}{dx} = A - \frac{BC}{C^2z^2 + 1} \tag{2}$$

and, as can be seen in Fig. (3) (b), this shows agreement with the stiffness data.

It is of note that the force-displacement shown here is fitted by the smooth function of Eq. (1), and is therefore quite unlike the complex, multi-event responses reported previously by Potter [28], Pirrera [31], Diaconu [30] and Shaw [32]. Although the numerous attachments to the plate will clearly influence its response, the multi-event snap is reproduced in [32] using a very similar method, so the change in behaviour may be attributed to the different choice of plate properties.

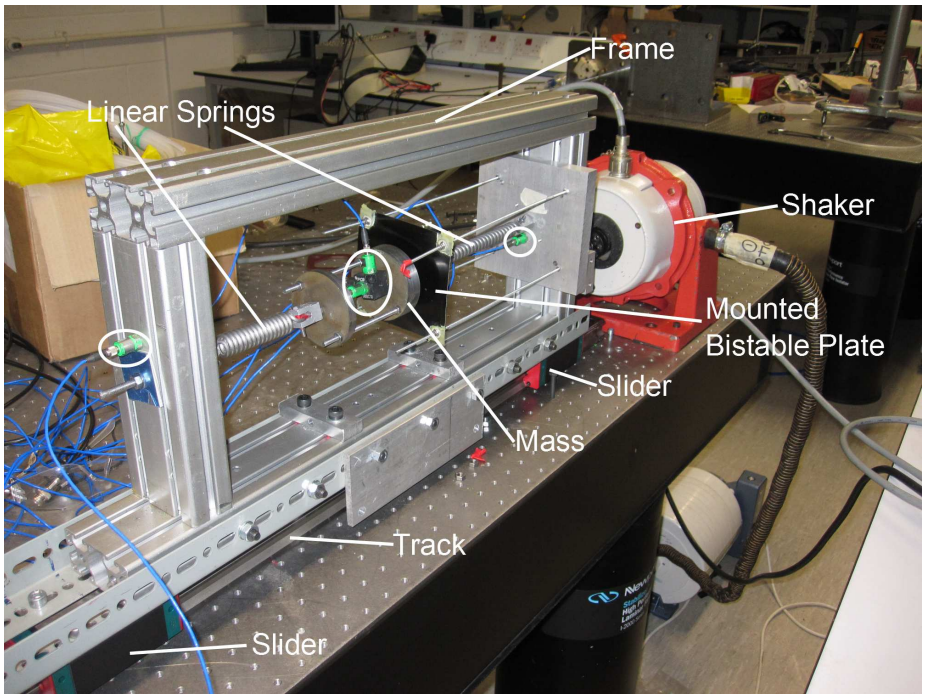

Figure 4: The assembled dynamic test rig. Circles show locations of accelerometers.

3. Dynamic response of a nonlinear mass-spring system incorporating the bistable plate subjected to base excitation

3.1. Experimental design

3.1.1. Dynamic test apparatus

The plate and mounting mechanism were incorporated into a dynamic test rig as shown in Fig. (4). The mass was suspended between two springs, that were tensioned such that they approximately horizontal. The centre of the bistable plate was attached with nuts to a threaded bar connected to the mass and springs. The position at which the plate was connected to the threaded bar was adjusted, until the plate was held in its mid-snap position by the relative tension in the two springs.

The outer frame slid upon cars on the steel track, which allowed no detectable rotation or lateral free play, whilst giving minimal axial friction. The

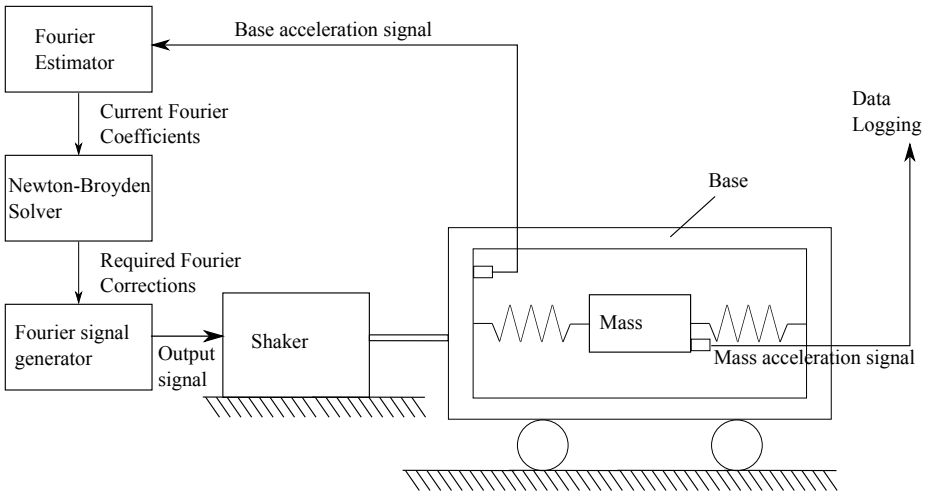

Figure 5: Schematic of experiment and control system.

frame was connected to a Ling V406 Shaker, by a connection which included a short laterally flexible element, which eliminated issues arising from small misalignments between the shaker and track.

The frame was designed to be far more rigid than the enclosed spring system; random noise tests were used to verify that no frame modes occurred within the frequency range of interest, and during testing accelerometers measured both the top and bottom of the frame, to ensure it was moving as a rigid body. Two more accelerometers were located on the mass, to check that no significant lateral motions occurred.

The combined stiffness of the linear springs k_{spring} was estimated as 33.8 N/mm by observing the natural frequency f of the mass-spring system with the plate decoupled, using $2\pi f = \sqrt{k_{spring}/m}$ with effective mass $m = 0.97$ kg.

3.1.2. Conditioning of the input signal

It was found that the nonlinearities in the system could influence the motion of the base, and cause distortions to the desired harmonic oscillation. For this reason, DSpace software and hardware and a Simulink® model were used to develop a control system that could minimise these unwanted harmonics. A

feed-forward system was used in preference to a feedback control system, to avoid potential issues of instability. The controller repeatedly sampled a buffer of data from the base accelerometer, then calculated the Fourier series of this signal based upon the required fundamental frequency, including terms up to the 5th harmonic. A numerical routine was run that assumed that the magnitude of each harmonic of the base signal was an unknown function of the output Fourier coefficients at the same harmonic, and used a Newton-Broyden algorithm to set them to zero, or the required amplitude in the case of the fundamental. A schematic of this system is shown in Fig. (5). In this way, the mean magnitudes of the first 5 harmonics were reduced to no more than 3% of the required fundamental amplitude.

It was found that the signal conditioning had little effect on the results presented here compared to results taken with an uncorrected signal, so long as the fundamental amplitude was controlled accurately, suggesting insensitivity to harmonic distortions.

3.1.3. Post processing

For each excitation frequency data point shown, a ten-second block of time series data was saved, for all accelerometers. These time series were then integrated twice to obtain a displacement signal, and a Fourier series was calculated and averaged for all complete cycles, with the known forcing frequency as the fundamental. This gave the absolute fundamental amplitude X, and the relative fundamental amplitude U could be found by subtracting the base displacement from the mass displacement and performing a similar process on the result.

3.2. Dynamic results

Fig. (6) shows detailed frequency response results at each of the four excitation amplitudes tested. Results were generally highly repeatable, with the main source of scatter appearing to be small changes of system properties during the period of testing.

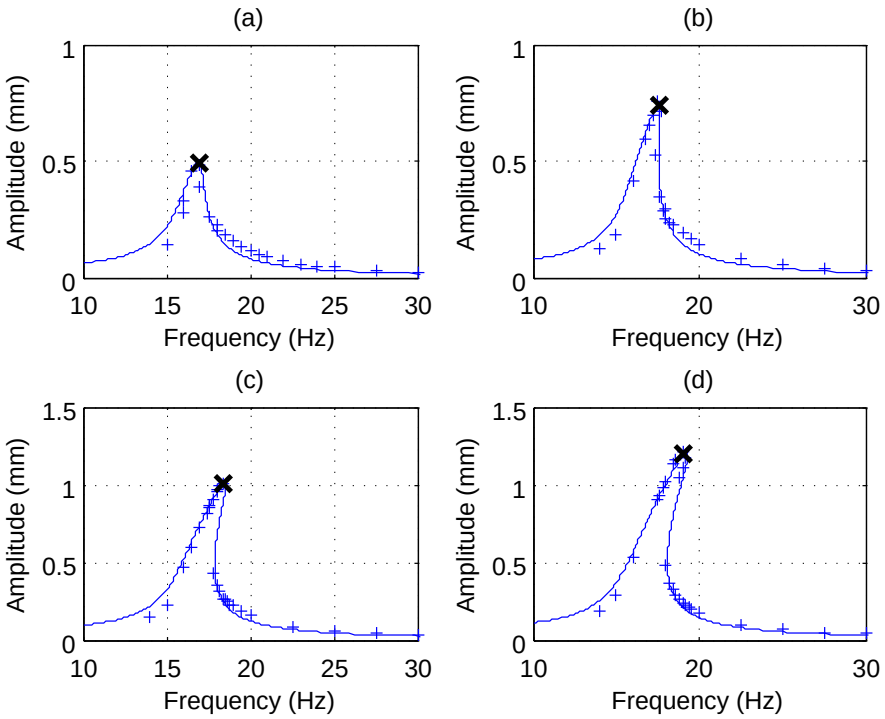

Figure 6: Fundamental absolute response amplitude for different values of base amplitude R and frequency. Crosses (+) show experimental data, peak values shown with (×), solid line shows response calculated in Section 5.3. (a) $R = 0.04$ mm (b) $R = 0.05$ mm (c) $R = 0.06$ mm (d) $R = 0.07$ mm

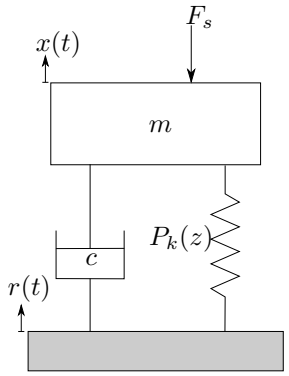

Figure 7: Mass m with static load F_s is supported on a movable base by a nonlinear spring with linear damper with damping constant c. $r(t)$ denotes base motion, $x(t)$ denotes displacement response of the mass and the nonlinear spring has force/displacement function $P_k(z)$.

4. Static and dynamic analysis of an HSLDS mount

To model the results, we provide a brief theoretical description of the HSLDS mount, summarising recent work by the authors [3]. Fig. (7) shows the system considered; a mass m subject to static load F_s is supported above a base by a nonlinear spring with force/displacement response $P_k(z)$ and linear damper with coefficient c. It is excited by base excitation signal $r(t)$, resulting in an absolute displacement from the static equilibrium position $x(t)$. Inspection of Fig. (7) gives the following equation of motion:

$$m\ddot{z} + c\dot{z} + P(z) = m\ddot{r} \tag{3}$$

where $z \equiv x(t) - r(t)$ and is known as relative displacement, $P(z) = F_s - P_k(z)$ and it is assumed that $z = 0$ at static equilibrium.

An HSLDS function for the nonlinear spring $P(z)$ is an odd function similar in form to Fig. (8) (a). Stiffness is low near the origin, giving reduced natural frequency at small amplitudes, while greater stiffness elsewhere minimises the deflection due to F_s. The equivalent linear system is defined as the linear system that has the same static displacement z_s at the given static load F_s, with consequent static stiffness $k_s \equiv F_s/z_s$. Distance and force are nondimensionalised by the static values; $\hat{x} = x/z_s$, $\hat{r} = r/z_s$, $\hat{z} = z/z_s$ and $\hat{P}(\hat{z}) = P(z_s\hat{z})/F_s$, giving

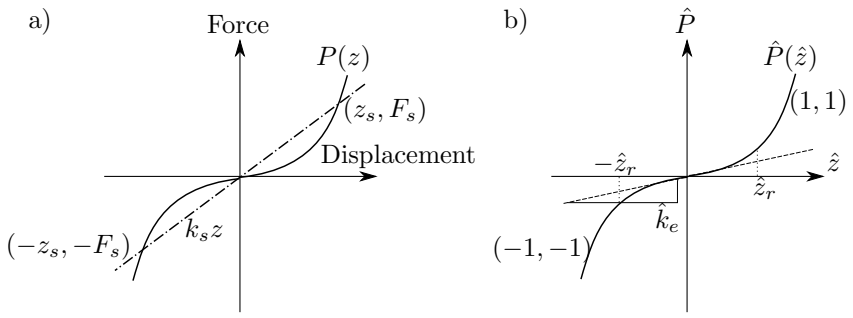

Figure 8: a) Generic example of an HSLDS force-displacement response (solid line), and the linear equivalent response which shares the same static displacement z_s and static force F_s, and has equivalent linear stiffness k_s (dot-dash line). b) Nondimensionalised system illustrating reduced stiffness range $\hat{z}_r$ and equilibrium stiffness $\hat{k}_e$.

the nondimensional response shown in Fig. (8) (b). Time is nondimensionalised by the natural frequency of the equivalent linear system $\omega_e \equiv \sqrt{k_s/m}$ to give $\tau \equiv t\omega_e$, and when all nondimensionalisations are substituted Eq. (3) becomes:

$$\hat{z}'' + 2\lambda\hat{z}' + \hat{P}(\hat{z}) = \hat{r}'' \tag{4}$$

where the prime $'$ denotes differentiation with regard to τ, and the damping ratio of the equivalent linear system is given by $\lambda \equiv c/(2\sqrt{k_s m})$.

The nondimensional HSLDS profile is characterised by two properties known as the equilibrium stiffness $\hat{k}_e$ and reduced stiffness range $\hat{z}_r$ as shown in Fig. (8) (b). Equilibrium stiffness is the nondimensional tangent stiffness at the equilibrium point:

$$\hat{k}_e \equiv \left.\frac{d\hat{P}}{d\hat{z}}\right|_{\hat{z}=0} \tag{5}$$

Reduced stiffness range is the range of $\hat{z}$ over which the stiffness is less than static stiffness k_s such that:

$$\left.\frac{d\hat{P}}{d\hat{z}}\right|_{|\hat{z}|<\hat{z}_r} < 1 \tag{6}$$

A 5th order polynomial response of form:

$$\hat{P}(\hat{z}) = k_1\hat{z} + k_3\hat{z}^3 + k_5\hat{z}^5 \tag{7}$$

can be fitted to match the condition that $\hat{P}(1) = 1$, and solved to satisfy Eq. (5)

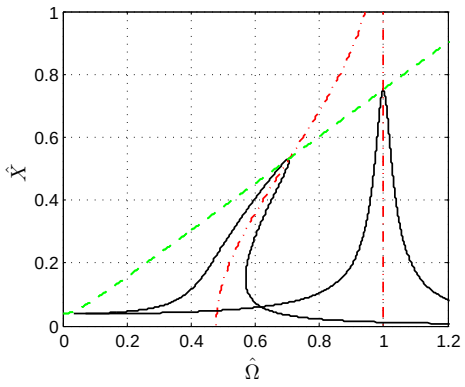

Figure 9: Typical absolute frequency response functions for an HSLDS mount. The right hand peak shows the response of the equivalent linear system for comparison. The dashed line shows the limit curve for the applied base excitation amplitude and damping, the dot-dash lines show backbone curves.

and Eq. (6) to obtain:

$$k_1 = k_e \ , \ k_3 = (1-\hat{k}_e)\frac{5\hat{z}_r^4 - 1}{5\hat{z}_r^4 - 3\hat{z}_r^2} \ , \ k_5 = (1-\hat{k}_e)\frac{1-3\hat{z}_r^2}{5\hat{z}_r^4 - 3\hat{z}_r^2} \tag{8}$$

This can give any choice of $\hat{k}_e$ although the choice of reduced stiffness range must be restricted to $\sqrt{1/5} \leq \hat{z}_r \leq \sqrt[4]{1/5}$ for realistic results. Dynamic simulation shows that for non-polynomial HSLDS functions, approximating the force-displacement curve using equations (5) to (8) gives very similar results [3].

To obtain the steady state response to harmonic base motion of the form $\hat{r} = \hat{R}\cos(\hat{\Omega}\tau + \phi)$, the method of Normal Forms [34, 35] is used in [3], however the Harmonic Balance method [36] would give identical results in this case. The method of Normal Forms assumes a relative response of the form $\hat{z} = \hat{U}\cos(\hat{\Omega}\tau) + \hat{h}(\tau)$, where $\hat{h}(\tau)$ is a small function containing harmonic responses that is neglected in this work. This results in a response equation that may be solved to find $\hat{U}$, the amplitude of the response at the forcing frequency :

$$\hat{\Omega}^4(\hat{U}^2 - \hat{R}^2) + 2\hat{\Omega}^2\hat{U}^2\left[2\lambda^2 - K(\hat{U})\right] + K(\hat{U})^2\hat{U}^2 = 0 \tag{9}$$

where $K(\hat{U})$ is the amplitude dependant stiffness:

$$K(\hat{U}) = \hat{k}_e + \frac{3k_3\hat{U}^2}{4} + \frac{10k_5\hat{U}^4}{16} \tag{10}$$

When forcing and damping are assumed to be zero, Eq. (9) defines the amplitude dependant natural frequency of the system, known as the backbone curve:

$$\hat{\Omega} = \sqrt{K(\hat{U})} \tag{11}$$

At resonance, stiffness and inertial terms cancel from Eq. (9) to give:

$$\hat{U} = \frac{\hat{\Omega}\hat{R}}{2\lambda} \tag{12}$$

which is known as the limit curve. The peak response for any given nonlinear spring occurs when its backbone curve intersects the limit curve for the relevant base amplitude and damping.

We are often primarily concerned with the absolute response of the payload mass. The nondimensional absolute fundamental magnitude $\hat{X}$ may be calculated from the relative magnitude $\hat{U}$ by

$$\hat{X} = \sqrt{(\hat{U} + \hat{R}\cos\phi)^2 + (\hat{R}\sin\phi)^2} \tag{13}$$

where ϕ is the phase angle between the base motion and relative response given by

$$\phi = \cos^{-1}\left(\frac{(-\hat{\Omega}^2 + K(\hat{U}))\hat{U}}{\hat{\Omega}^2\hat{R}}\right) \tag{14}$$

Eqns. (11) and (12) concern a system that is in resonance, so therefore $\phi = \pi/2$ and $\hat{U} >> \hat{R}$, and the effect of $\hat{R}$ becomes negligible in Eq. (13) so that $\hat{U} \approx \hat{X}$. Therefore limit curves and backbone curves are identical when plotted in terms of relative or absolute response, except at very low frequencies where $\hat{X} \to \hat{R}$.

An example response is shown in Fig. (9), showing that the use of an HSLDS mount reduces both the peak frequency and the peak amplitude of response to base excitation. Note that at low frequency, the absolute response magnitude converges to the base motion amplitude. Fig. (9) shows that the region where absolute response magnitude is less than that of the base magnitude, known as the isolation region, begins at much lower frequency for the HSLDS mount than for the equivalent linear system.

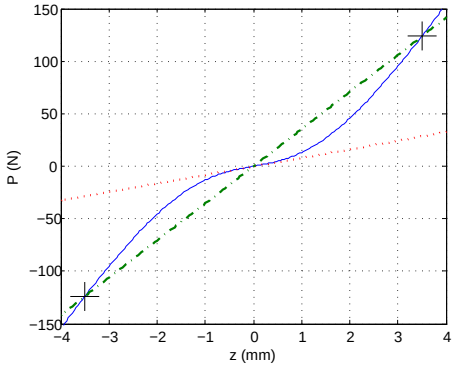

Figure 10: Total force displacement function given by Eq. (15) (solid). Dotted line gradient shows equilibrium stiffness, dot-dashed line shows equivalent linear system. Crosses indicate chosen static displacement and consequent static force.

5. Comparison of Experimental Data with Theory

5.1. Nondimensionalising the total response of plate and springs

The combined response of the linear spring and bistable plate, is found by summing them to obtain:

$$P(z) = (A + k_{spring})z - B\arctan(Cz) \tag{15}$$

This function is plotted in Fig. (10), along with the equilibrium stiffness k_e of 8.09 N/mm found by taking the derivative of Eq. (15) at $z = 0$. There is no actual static load of interest in our experiment, so a static displacement of z_s =3.5 mm is assumed, chosen because this value gives reasonable nondimensional properties as described below. Evaluating Eq. (15) at this value obtains F_s=123.8 N, and therefore static stiffness k_s=35.4 N/mm.

Nondimensionalising Eq. (15) as described in Section 4 therefore gives $\hat{k}_e = 0.229$ and $\hat{z}_r = 0.464$, where a numerical solver is used to satisfy Eq. (6); this allows a polynomial approximation to be calculated using Eqs. (7) and (8).

5.2. Comparison of Backbone curves

Fig. (11) shows all result sets shown in Fig. (6) nondimensionalised as described in Sections 4 and 5.1. Three backbone curves are shown in bold; the

dot-dashed backbone is calculated using Eqs. (8), (10) and (11) with the values of $\hat{k}_e$ and $\hat{z}_r$ calculated for Eq. (15) in Section 5.1. As can be seen, this curve has a qualitatively similar shape to the data but is inaccurate in terms of frequency. The reason for this is found by inspecting the inset in Fig. (3) (b) at z=0 mm; there is a range of approximately 2 N/mm in the data, and this is a significant proportion of the dimensional equilibrium stiffness, which is calculated to be 8.09 N/mm. Furthermore, it is likely that there is some error in adjusting the plate so that it is held at its exact centre. Therefore it is difficult to establish the true equilibrium stiffness value with accuracy. A value for the stiffness of the plate at z= 0mm of -23.5 N/mm, which Fig. (3) shows occurs inside a range of 0.5 mm from zero, gives a dimensional stiffness of 10.3 N/mm when summed with the spring stiffness. Nondimensionalising by the calculated static stiffness gives $\hat{k}_e = 0.291$, and this value in Eqs. (8), (10) and (11) gives the solid backbone curve in Fig. (11) which fits the data well. Finally, the dotted backbone curve shown in Fig. (11) shows the response if the model is simply taken to be a cubic polynomial with the same equilibrium stiffness, showing that this model fails to capture the shape of the backbone at higher amplitudes.

5.3. Experimental limit curves, damping estimation and full response

The peak response frequencies and amplitudes on Fig. (6) (marked with ×) can be used in Eq. (12) to predict damping constant λ, and therefore the associated limit curves may be calculated. However, the form of this equation implies that if damping is linear and constant, the limit curves will intercept the line $\hat{\Omega} = 1$ on Fig. (11) at heights proportional to their respective excitation amplitude. The results, circled on Fig. (11), do not show this prediction, for two reasons. Firstly, the peak values of the experimental graphs may not be entirely accurate; when response has a 'drop-down', it is not possible to know exactly how near to the true peak frequency was reached before the drop-down was triggered. Secondly, there is no physical reason for the assumption of linear damping, so some amplitude dependence may be occurring.

Nevertheless, the above method is used to calculate values of λ separately

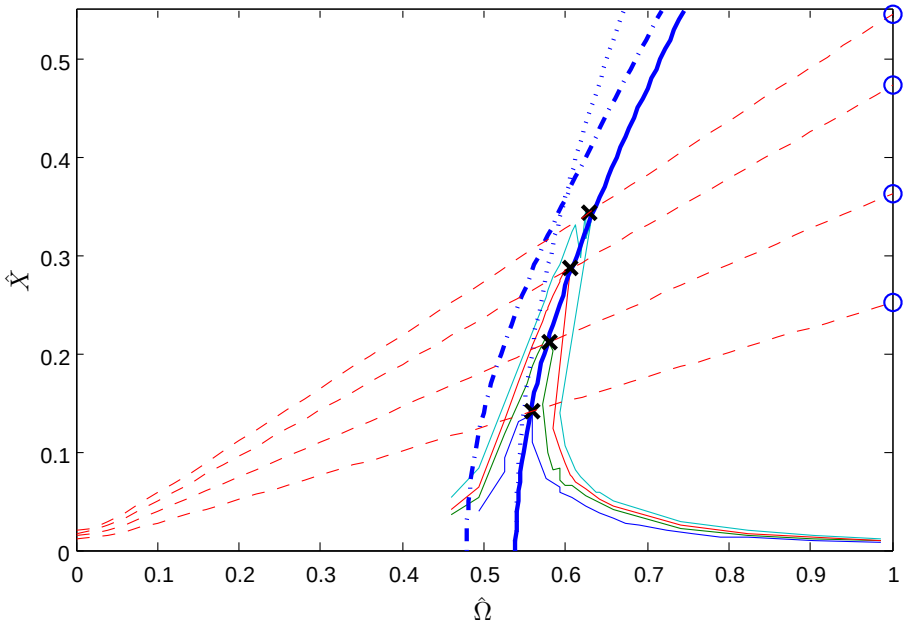

Figure 11: Nondimensionalised absolute frequency response, showing all datasets (thin solid lines). Dashed values show limit curves implied by peak values (×) assuming linear damping. Bold lines show backbone curves; dot-dash line shows calculated back bone response based on function Eq. (15), solid line uses a modified value for $\hat{k}_e$ and dotted line is the backbone implied by assuming a cubic response. Circles indicate the predicted peak response of the equivalent linear system.

for each different level of forcing. The solutions of Eq. (9) can then be found, converted to absolute response with Eq. (13), and plotted in dimensional form as solid lines on Fig. (6). This shows good agreement with experiment.

6. Conclusions

An experimental concept demonstrator for a passive vibration isolator incorporating a composite bistable plate has been built, and subjected to harmonic base excitation. Quasi-static tests have been performed to characterise the force-displacement properties of the snap through of the bistable plate, and the results used to make predictions for the dynamic response of a spring-mass system coupled with this plate.

The quasi-static results show that by selecting suitable plate parameters the force through of a bistable plate need not be the complex multi-stage event reported by other authors, although in this study the plate is incorporated in a mechanism that may affect the plate response.

The dynamic results show good agreement with theoretical predictions, in particular the backbone curve which matches the shape of the frequency response function well, although it proved difficult to accurately predict the equilibrium stiffness due to experimental scatter. Selecting the peak response at a given amplitude is not a particularly robust way to find the damping ratio of the system, and the assumption of linear damping could not be verified. However, deriving the damping ratio in this way and using it in our model to calculate the response away from the peak still gave reasonably accurate results.

Future work on this will move towards a more compact mounting, with a view towards achieving a simple, lightweight and highly effective means of isolating vibration.

Acknowledgements

The authors would like to thank Dr David Barton and Clive Rendall for their assistance in this project. Alexander Shaw has an EPSRC studentship from the Advanced Composites Centre for Innovation and Science (ACCIS) Doctoral Training Centre (DTC), grant number EP/ G036772/1. Simon Neild is an EPSRC research fellow.

References

[1] D. J. Mead, Passive Vibration Control, John Wiley and Sons, 1999.

[2] A. Carrella, Passive Vibration Isolators with High-Static-Low-Dynamic-Stiffness, VDM Verlag Dr. Muller, 2010.

[3] A. D. Shaw, S. A. Neild, D. J. Wagg, Dynamic analysis of high static low dynamic stiffness vibration isolation mounts, Journal of Sound and Vibration(to be published).

[4] R. Ibrahim, Recent advances in nonlinear passive vibration isolators, Journal of Sound and Vibration 314 (3-5) (2008) 371 – 452.

[5] M. W. Hyer, Some observations on the cured shape of thin unsymmetric laminates, Journal of Composite Materials 15 (2) (1981) 175–194.

[6] A. Carrella, M. Friswell, A. Pirrera, G. Aglietti, Numerical and experimental analysis of a square bistable plate, in: International Conference on Noise and Vibration (ISMA 2008), 2008.

[7] J. Winterflood, D. G. Blair, B. Slagmolen, High performance vibration isolation using springs in euler column buckling mode, Physics Letters A 300 (2-3) (2002) 122–130.

[8] L. N. Virgin, R. B. Davis, Vibration isolation using buckled struts, Journal of Sound and Vibration 260 (5) (2003) 965–973.

[9] R. H. Plaut, J. E. Sidbury, L. N. Virgin, Analysis of buckled and prebent fixed-end columns used as vibration isolators, Journal of Sound and Vibration 283 (3-5) (2005) 1216–1228.

[10] L. N. Virgin, S. T. Santillan, R. H. Plaut, Vibration isolation using extreme geometric nonlinearity, Journal of Sound and Vibration 315 (3) (2008) 721–731.

[11] S. T. Santillan, Analysis of the elastica with applications to vibration isolation, Ph.D. thesis, Department of Mechanical Engineering and Materials Science, Duke University (2007).

[12] R. DeSalvo, Passive, nonlinear, mechanical structures for seismic attenuation, Journal of Computational and Nonlinear Dynamics 2 (4) (2007) 290–298.

[13] A. Carrella, M. Brennan, T. Waters, Static analysis of a passive vibration isolator with quasi-zero-stiffness characteristic, Journal of Sound and Vibration 301 (301) (2007) 678 – 689.

[14] A. Carrella, M. Friswell, A. Zotov, D. Ewins, A. Tichonov, Using nonlinear springs to reduce the whirling of a rotating shaft, Mechanical Systems and Signal Processing 23 (7) (2009) 2228 – 2235.

[15] A. Carrella, M. Brennan, T. Waters, V. L. Jr., Force and displacement transmissibility of a nonlinear isolator with high-static-low-dynamic-stiffness, International Journal of Mechanical Sciences 55 (1) (2012) 22 – 29.

[16] I. Kovacic, M. J. Brennan, T. P. Waters, A study of a nonlinear vibration isolator with a quasi-zero stiffness characteristic, Journal of Sound and Vibration 315 (3) (2008) 700 – 711.

[17] N. Zhou, K. Liu, A tunable high-static low-dynamic stiffness vibration isolator, Journal of Sound and Vibration 329 (9) (2010) 1254 – 1273.

[18] W. S. Robertson, M. R. F. Kidner, B. S. Cazzolato, A. C. Zander, Theoretical design parameters for a quasi-zero stiffness magnetic spring for vibration isolation, Journal of Sound and Vibration 1-2 (2009) 88–103.

[19] T. D. Le, K. K. Ahn, A vibration isolation system in low frequency excitation region using negative stiffness structure for vehicle seat, Journal of Sound and Vibration 330 (26) (2011) 6311–6335.

[20] M. W. Hyer, Calculations of the room-temperature shapes of unsymmetric laminates, Journal of Composite Materials 15 (1981) 296–310.

[21] C. G. Diaconu, P. M. Weaver, F. Mattioni, Concepts for morphing airfoil sections using bi-stable laminated composite structures, Thin-Walled Structures 46 (6) (2008) 689 – 701.

[22] M. R. Schultz, A concept for airfoil-like active bistable twisting structures, Journal of Intelligent Material Systems and Structures 19 (2) (2008) 157–169.

[23] A. Gatto, F. Mattioni, M. Friswell, Experimental investigation of bistable winglets to enhance wing lift takeoff capability, Journal of Aircraft 46 (2) (2009) 647.

[24] S. Daynes, P. Weaver, K. Potter, P. Margaris, P. Mellor, Bistable composite flap for an airfoil, Journal of Aircraft 47 (2010) 334–338.

[25] S. Daynes, P. Weaver, J. Trevarthen, A morphing composite air inlet with multiple stable shapes, Journal of Intelligent Material Systems and Structures 22 (9) (2011) 961–973.

[26] X. Lachenal, S. Daynes, P. M. Weaver, Review of morphing concepts and materials for wind turbine blade applications, Wind Energy(to be published).

[27] M. Dano, M. W. Hyer, The response of unsymmetric laminates to simple applied forces, Mechanics of Composite Materials and Structures 3 (1) (1996) 65–80.

[28] K. Potter, P. Weaver, A. Seman, S. Shah, Phenomena in the bifurcation of unsymmetric composite plates, Composites Part A: Applied Science and Manufacturing 38 (1) (2007) 100 – 106.

[29] S. Tawfik, X. Tan, S. Ozbay, E. Armanios, Anticlastic stability modeling for cross-ply composites, Journal of composite materials 41 (11) (2007) 1325–1338.

[30] C. G. Diaconu, P. M. Weaver, A. F. Arrieta, Dynamic analysis of bi-stable composite plates, Journal of Sound and Vibration 322 (4-5) (2009) 987 – 1004.

[31] A. Pirrera, D. Avitabile, P. Weaver, Bistable plates for morphing structures: A refined analytical approach with high-order polynomials, International Journal of Solids and Structures 47 (25-26) (2010) 3412 – 3425.

[32] A. D. Shaw, A. Carrella, Force displacement curves of a snapping bistable plate, in: Proceedings of the 30th IMAC, A Conference on Structural Dynamics, 2012, pp. 191–198.

[33] S. Daynes, P. M. Weaver, Analysis of unsymmetric cfrp-metal hybrid laminates for use in adaptive structures, Composites Part A: Applied Science and Manufacturing 41 (11) (2010) 1712–1718.

[34] S. A. Neild, D. J. Wagg, Applying the method of normal forms to second-order nonlinear vibration problems, Proc. R. Soc. A 467 (2128) (2010) 1141 – 1163.

[35] S. A. Neild, Approximate methods for analysing nonlinear structures, in: L. Virgin, D. Wagg (Eds.), Exploiting Nonlinear Behaviour in Structural Dynamics, Springer, 2012, pp. 53 – 109.

[36] D. Wagg, S. Neild, Nonlinear Vibration with Control, Springer, 2009.